Growth of High-Quality Centimeter-Size Single-Crystal Graphene on High-Temperature Annealed Cu (111) Substrate

QI Jianhai[1,2], *CHEN Yang*[1,2], *YUE Yuanyuan*[3], *LYU Bingchen*[1,2], *CHENG Yuang*[1,2], *ZHU Fengqian*[1,2], *JIA Yuping*[1,2], *LI Shaojuan*[1,2], *SUN Xiaojuan*[1,2], *LI Dabing*[1,2]

(1. State Key Laboratory of Luminescence and Applications, Changchun Institute of Optics, Fine Mechanics and Physics, Chinese Academy of Sciences, Changchun 130033, China; 2. Center of Materials Science and Optoelectronics Engineering, University of the Chinese Academy of Sciences, Beijing 100049, China; 3. School of Management Science and Information Engineering, Jilin University of Finance and Economics, Changchun 130117, China)

Abstract: Two-dimensional (2D) graphene has shown great potential of breakthrough of Moore's law limitation due to its atomic thickness in electronic devices. Up to now, chemical vapor deposition (CVD) is a widely applied method for graphene growth due to its low-cost, large-area production, and easy control in layer number. However, the CVD-grown graphene usually suffers from relatively low quality derived from the polycrystalline nature of catalytic metal (e.g., Cu) substrates. Herein, single-crystal Cu (111) substrates were fabricated by a high-temperature annealing process, initial nucleation of graphene on it has been well controlled, and high-quality and centimeter-size single-crystal graphene was achieved. The Cu (111) substrate provides onefold orientation for the graphene growth according to their lattice matching relation, and domain boundaries of neighboring graphene nuclei could stitch together. The as-grown single-crystal graphene has an average sheet resistance of 607.5 $\Omega \cdot sq^{-1}$. Compared to that of grown on the pristine polycrystalline Cu (1 415.7 $\Omega \cdot sq^{-1}$), it shows high electrical conductivity. High-temperature annealing purified the Cu foils, and induced a clean graphene surface with lower roughness. The quality of graphene is further verified by using it in a field-effect transistor (FET), resulting in a maximum switch ratio of 145.5 and carrier mobility of 2.31×10^3 $cm^2 \cdot V^{-1} \cdot s^{-1}$. Based on these results, we believe that the single-crystal graphene in present work is also feasible for fabricating other high-performance electronic devices.

Key words: Cu (111); graphene; high-temperature annealing; chemical vapor deposition; field-effect transistor

CLC number: O782$^+$.7 **Document code**: A **Article ID**: 1000-985X(2023)11-1980-09

DOI:10.16553/j.cnki.issn1000-985x.20231011.001

高温退火 Cu (111)衬底上生长高质量厘米尺寸单晶石墨烯

祁建海[1,2],陈 洋[1,2],岳圆圆[3],吕炳辰[1,2],程宇昂[1,2],朱凤前[1,2],贾玉萍[1,2],李绍娟[1,2],孙晓娟[1,2],黎大兵[1,2]

(1. 中国科学院长春光学精密机械与物理研究所,发光及应用国家重点实验室,长春 130033;
2. 中国科学院大学,材料科学与光电工程中心,北京 100049;3. 吉林财经大学管理科学与信息工程学院,长春 130117)

摘要:二维(2D)石墨烯具有原子层厚度,在电子器件中展示出突破摩尔定律限制的巨大潜力。目前,化学气相沉积(CVD)是一种广泛应用于石墨烯生长的方法,满足低成本、大面积生产和易于控制层数的需求。然而,由于催化金属

Received date: 2023-04-13

Foundation items: National Key R&D Program of China (2021YFB3601600); National Natural Science Foundation of China (61827813, 52002368, 62121005, 62074147, 62022081, 61974099); Natural Science Foundation of Jilin Province (20230101345JC, 20230101107JC, 20230508132RC); Youth Innovation Promotion Association of the Chinese Academy of Sciences (Y201945, 2019222)

Biography: QI Jianhai (1995—), male, from Jiangsu Province, master. E-mail: 2603591798@qq.com

Corresponding author: CHEN Yang, associate researcher. E-mail: cheny@ciomp.ac.cn
SUN Xiaojuan, researcher. E-mail: sunxj@ciomp.ac.cn

(例如 Cu)衬底一般为多晶特性,导致 CVD 法生长的石墨烯晶体质量相对较差。为此,通过高温退火工艺制备了 Cu (111)单晶衬底,使石墨烯的初始成核过程得到了很好的控制,从而实现了厘米尺寸的高质量单晶石墨烯的制备。根据二者的晶格匹配关系,Cu (111)衬底为石墨烯生长提供了唯一的成核取向,相邻石墨烯成核岛的边界能够缝合到一起。单晶石墨烯具有高电导率,相较于原始多晶 Cu 上生长的石墨烯(1 415.7 $\Omega \cdot sq^{-1}$),其平均薄层电阻低至 607.5 $\Omega \cdot sq^{-1}$。高温退火能够清洁铜箔,从而获得表面粗糙度较低的洁净石墨烯。将石墨烯用于场效应晶体管(FET),器件的最大开关比为 145.5,载流子迁移率为 2.31×10^3 $cm^2 \cdot V^{-1} \cdot s^{-1}$。基于以上结果,相信本工作中的单晶石墨烯还满足其他高性能电子器件的制备。

关键词:Cu (111);石墨烯;高温退火;化学气相沉积;场效应晶体管

0 Introduction

Since two-dimensional (2D) graphene was firstly prepared by Novoselov et al. in 2004[1], it has been developed rapidly due to its excellent mechanical strength[2], high carrier mobility[3] and thermal conductivity[4]. The electronic devices based on graphene, for example graphene field-effect transistor (G-FET), show high operation speed and carrier mobility. Meanwhile, the atomic thickness of graphene might break the limitation of Moore's law. Currently, the chemical vapor deposition (CVD) method is widely applied for the growth of graphene and other 2D materials[5-6], showing unique advantages of low-cost, large-area production, and easily controlled properties compared to mechanical exfoliation[7] and liquid-phase exfoliation[8-11]. However, the as-grown graphene by CVD method still faces a great challenge of relatively low crystalline quality derived from the polycrystalline catalytic Cu substrate. The polycrystalline Cu may cause chaotic orientation of graphene nucleation and induce numerous defects and grain boundaries[12-13].

Up to now, the Cu foils are widely severed as the catalytic metal substrate for graphene growth for its excellent catalytic ability, easy availability and proper epitaxial relationship with graphene[14]. The CVD-grown mechanism of graphene on Cu substrate is known as a surface catalytic process because of its low carbon species solubility[15-16]. When the precursor (e.g., CH_4) is decomposed in the presence of catalyst Cu at high temperature, the carbon atoms would be adsorbed on the Cu surface and arranged into hexagonal structure by the lattice field action of underneath Cu substrate. Therefore, the lattice matching between graphene and Cu substrate determines the initial nucleation orientation, implying that the crystalline properties of Cu are crucial for high-quality graphene growth. The single-crystal Cu (111) possesses a hexagonal symmetry, which perfectly matches with the graphene lattice, and may confine the graphene nuclei in one and only orientation[17].

Direct high-temperature annealing of polycrystalline metals is a generally used method to improve their crystalline quality[18-19]. The crystal orientation transformation and grain boundary mergence may happen during the annealing process. In previous works, the high-temperature annealing of suspending metal foils[19], introducing single-crystal seed[20], and making slits in metal foils[21] are proposed to produce their single-crystal formation in large size. However, these unavoidable preconditions restricted the preparation of single-crystal metals, and made the preparation process more complicated. Here, a simple annealing method needs to be further explored and investigated for preparing single-crystal Cu (111) substrate, which would facilitate the advances of high-quality growth of graphene and fabrication of high-performance electronic devices.

In this work, single-crystal Cu (111) catalytic substrate is obtained from its pristine polycrystalline state by an optimized high-temperature annealing process. The length of Cu foil is 5 cm. By carefully regulating the annealing conditions, the surface morphology of Cu becomes much flatter and smoother. The initial nucleation orientation of graphene on Cu (111) is in orderly arrangement because of their onefold lattice matching relation, and thus centimeter-size single-crystal graphene layer is achieved. The graphene grown on annealed single-crystal Cu (111) shows decreased residues and pollution, with an optimized root-mean-square roughness (Ra) of 1.41 nm. Besides, the high quality of graphene is verified by the minor oxidation of underneath catalytic Cu foils, low sheet resistance,

and weak intensity of defect-related D band in Raman spectra/mapping measurement. The G-FET is fabricated to further evaluate the electrical properties of single-crystal graphene.

1 Experimental section

1.1 High-temperature annealing of Cu foils

The 25 μm-thick Cu foils purchased from Jin Ding Metals were pretreated by HCl solution (10%, volume fraction) to remove the oxidized layer, then, cleaned by deionized (DI) water and dried by N_2 gun[22]. The pretreated Cu foils were cut into square sheets each with a size of 5 cm × 5 cm, and placed in a half quartz tube with the diameter of 5 cm. The quartz tube with Cu foils was placed into a low-pressure CVD (LPCVD) system (BEQ, Anhui Best Equipment Technology Co., Ltd., China), just locating at the middle area of the heating box. The annealing chamber was evacuated to ~6 Pa for venting the air, and 50 mL/min Ar and 10 mL/min H_2 were put in for providing protection and reduction environment for Cu annealing, corresponding to a pressure of ~56.7 Pa. The Cu foils were annealed at a temperature of 1 060 ℃ for 3 h, and slowly dropped to room temperature by ~4 h. It should be noted that the annealing conditions of temperature, time, and Ar/H_2 flux were carefully controlled and investigated.

1.2 Growth and transfer of graphene and fabrication of G-FET

The annealed Cu foils were used as the catalytic substrate for graphene growth, and the pristine polycrystalline Cu severed as the reference. The graphene growth was subsequently carried out in the LPCVD system. 100 mL/min Ar as carrier gas, 5 ~ 50 mL/min H_2 as reduction gas, and 1 ~ 3 mL/min CH_4 as carbon source were put in, and the growth temperature was maintained at 1 000 ℃. In order to observe the nucleation and coalescence processes, the growth of graphene was interrupted at the timeline of 5, 15 and 40 min. After the growth, the samples were rapidly cooled to room temperature within 1 h by directly removing the heating box and exposing the region of samples to the surrounding environment.

For further evaluation, the graphene was transferred onto dielectric substrates (e. g., Si/SiO_2) by a previously reported S1805G polymer-assisted wet transfer strategy[23]. The S1805G polymer was spin-coated onto the front graphene on Cu, and the backside graphene was etched away by Ar plasma. The chemical etching of Cu consists of two steps, one is rapid in which the etchant of H_2O_2 & HCl mixture solution is applied, and the other is the slow in which $Na_2(SO_4)_2$ solution was applied. Then, the graphene/S1805G was cleaned by DI water and transferred onto the dielectric substrate. After drying in air, the S1805G polymer was removed in hot organic solvent, leaving the graphene layer on the substrate.

The G-FET was fabricated by depositing a pair of Ti/Au electrodes via the widely used "lift-off" method, 10 nm Ti and 50 nm Au were evaporated by electron beam evaporation and thermal vacuum evaporation, respectively. The evaporation rate and chamber pressure are controlled to be 0.5 Å · s^{-1} and less than 5×10^{-4} Pa. Since the high-temperature treatment of graphene may cause additional damage, none metal electrode annealing is applied, which could maintain the pristine quality of graphene.

1.3 Characterization and measurement

The crystalline properties of Cu foils were evaluated by X-ray diffraction (XRD, D8 Focus, Bruker, Germany). Raman spectrophotometer (LabRAM HR Evolution, HORIBA Scientific, UK) with a 532 nm excited laser was applied to measure the Raman spectra and mapping of graphene. The surface morphology of Cu oxidization and transferred graphene were measured by scanning electron microscope (SEM, S-4800, Hitachi, Japan) and atomic force microscopy (AFM, MULTI MODE 8, Bruker, Germany). The large structures of the surface of Cu foils were observed by optical microscope (OM, DS-Ri2, Nikon, Japan). The sheet resistance of graphene was obtained by 4-probe resistivity measurement system (RTS-8, 4 Probes Tech, China).

The output characteristic and transfer characteristic curves of G-FET were measured by a semiconductor tester

(FS-Pro, Shenzhen Cindbest Technology Co., Ltd., China).

2 Results and discussion

2.1 Preparation of single-crystal Cu (111) by high-temperature annealing

The schematic diagrams of Cu annealing, graphene growth and transfer are shown in Fig. 1(a) ~ (f), the details are illustrated in the above. The inset in Fig. 1(d) reveals that the lattice of Cu (111) is perfectly matched with the hexagonal structure of graphene. After annealed at 1 060 ℃ for 3 h (see Fig. 1(g)), the Cu foil was etched by $Na_2(SO_4)_2$ solution to raise the grain boundaries, and the pristine Cu is used as the reference. The photos of the etched Cu foils are shown in Fig. 1(h) (pristine Cu) and Fig. 1(i) (annealed Cu). There are numerous flashy spots in the pristine Cu, which belong to the different orientation of Cu crystalline domains. However, the annealed Cu exhibits uniform morphology, and the domain boundaries obviously decreased. It should be noted that the uniformity of the annealed Cu has covered its full length of 5 cm.

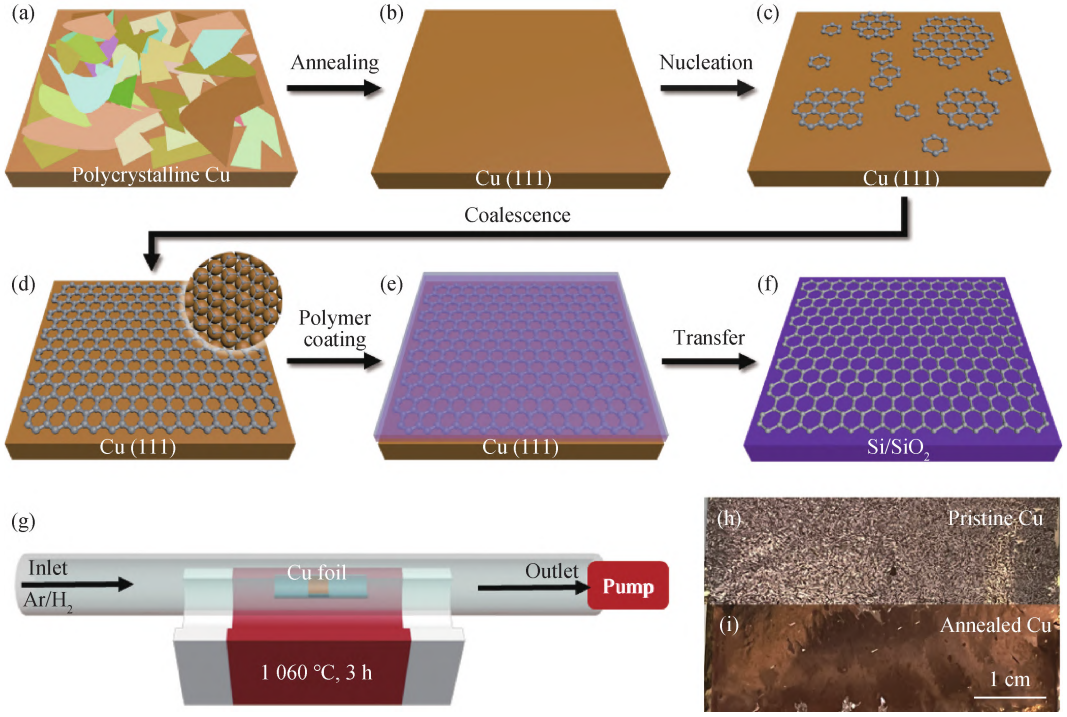

Fig. 1 Fabrication of large-area Cu (111) substrate and growth of single-crystal graphene. Schematic diagrams of high-temperature Cu annealing (a), (b), graphene growth (c), (d) and transfer processes (e), (f). The inset of (d) is the lattice matching relation of graphene on the Cu (111). (g) Configuration of annealed Cu foils in the chamber of LPCVD system. (h) Digital photos of the pristine Cu and (i) annealed Cu foils after the chemical etching

As shown in Fig. 2(a), there are numerous one-dimensional (1D) ridges on the pristine Cu foils, which were induced during the manufacturing process named as metallurgical cold rolling[24]. In this process, the rolling temperature is much lower than that of the melting point of Cu, and the hard scraping with roller pins would imprint 1D ridges on Cu foils. After high-temperature annealing, these ridges were eliminated, resulting in smoother surface morphology as shown in Fig. 2(b). These results are further evaluated by the AFM images in Fig. 2(c) and (d), and the height profiles extracted from AFM images are shown below. The maximum height fluctuation of the pristine Cu foil is ~40 nm, which is much higher than that of annealed Cu foil (~15 nm). Besides, well-organized step structures are observed for the annealed Cu foil in Fig. 2(d), as marked by the dashed lines. These structures are recognized as bunched step-edges on the annealed Cu foils, which was also reported in the previous work[25-26]. The step-edges with widths of several hundred nanometers are bunched by numerous atomic steps,

which were generated during the cooling process of Cu annealing by the surface reconstruction process.

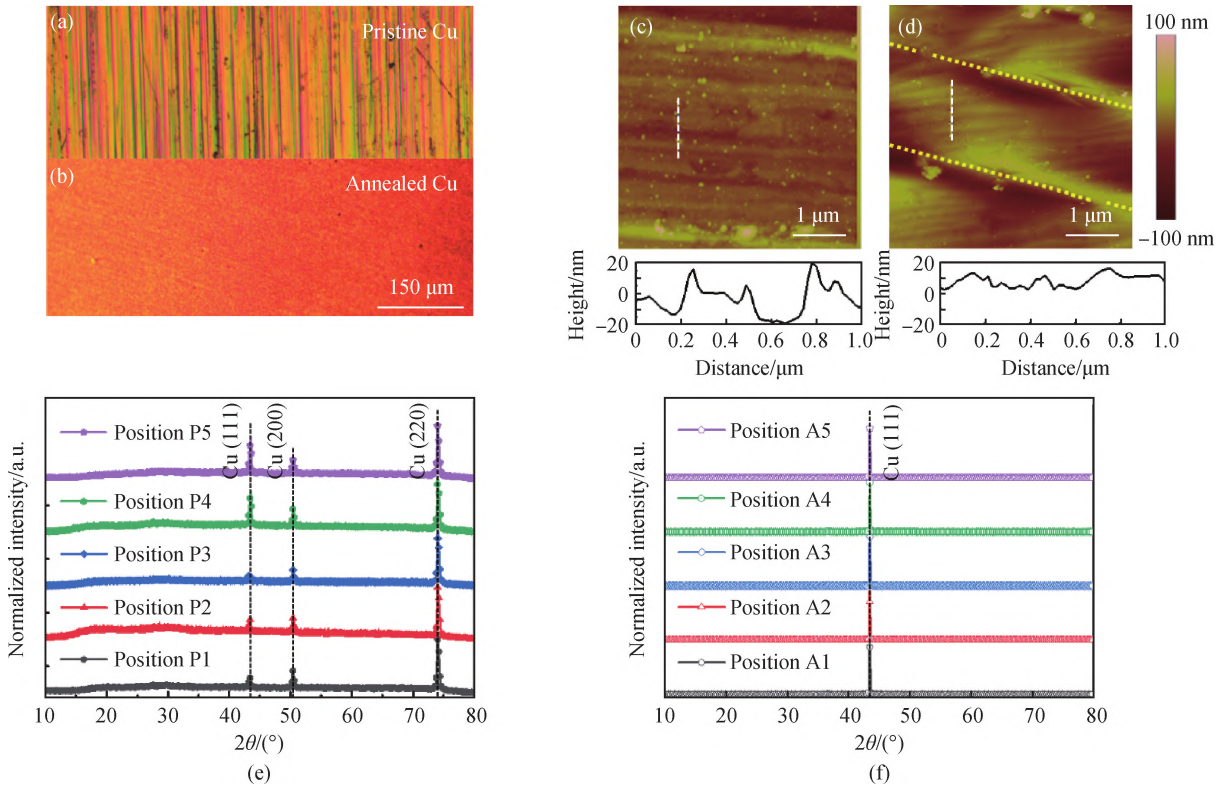

Fig. 2　Characterization and comparison of pristine Cu foils and high-temperature annealed single-crystal Cu (111) foils. OM images (a) and AFM images (c) of pristine Cu foils and annealed Cu foils (b), (d). The bottom of (c) and (d) is height profile extracted from the AFM images, these positions are marked by the white dashed lines. XRD 2θ scans of pristine Cu foils (e) and annealed Cu foils (f), five positions are selected for each sample

The surface morphology variations of annealed Cu foils after different annealing time (1, 2 and 3 h) are measured and compared. It is found that the planarization of Cu foils is progressive, and the 1D ridges gradually decrease with the annealing time increasing. In addition, the domain boundaries still exist for Cu foils annealed for 1 and 2 h, and the domain boundary density decreases for longer annealing time. For 3 h annealing, both of the 1D ridges and domain boundaries are eliminated, which is consistent with the results shown in Fig. 2(b) and (d). These results indicate that the annealing time of 3 h is enough for optimizing the surface morphology of Cu foils in present work.

2θ scans in XRD patterns are applied to evaluate the crystalline properties of Cu, as shown in Fig. 2(e) and (f), five positions on the pristine Cu (P1 ~ P5) and annealed Cu (A1 ~ A5) are selected. The polycrystalline nature of pristine Cu is revealed by the multiple crystal plane diffraction peaks of Cu (111), Cu (200), and Cu (220)[27] for the five measured positions. As a comparison, the Cu foils annealed at 1 060 ℃ for 3 h exhibits only one peak related to Cu (111) crystal plane. The uniform diffraction peaks for these measured positions proved the consistent out-of-plane Cu (111) orientation. In addition, the chemical etching of annealed Cu foils in Fig. 1(i) shows nearly none domain boundary, demonstrating the uniformity of in-plane orientation. Therefore, it could be concluded that the single-crystal Cu (111) is obtained by the high-temperature annealing process. It is known that the Cu (111) crystal plane in the face-centered cubic metal is the most thermodynamically stable, thus, atoms would tightly pack along this plane during the annealing process[28].

2.2　Nucleation and growth of graphene on single-crystal Cu (111)

The nucleation and growth behaviors of graphene on pristine polycrystalline Cu and annealed single-crystal Cu

(111) are compared, and corresponding SEM images at certain growth timelines are shown in Fig. 3(a) and (b). In order to make the graphene layer on Cu more obvious, the as-grown samples are oxidated in air by heating, during which CuO_x generated at the area without the graphene coverage. For the initial growth time of 5 min, high-density graphene nucleation with a random distribution occurs on the pristine polycrystalline Cu, it is recognized that the irregular 1D ridges and domain boundaries of pristine Cu foils provide nucleation sites for graphene growth[29]. As for the single-crystal Cu (111), the graphene has lower nucleation density and larger size, meanwhile, the orientation of graphene nuclei follows exactly the same direction, as marked by the dashed lines. As the growth time going for 15 and 40 min, the graphene has merged into a continuous film. After oxidation of Cu foils, lots of CuO_x particles (e.g., typical white dots marked by solid lines) generate over the graphene layer grown on pristine polycrystalline Cu, implying that there are many detects for oxygen permeation. As a comparison, no obvious oxidation of annealed single-crystal Cu (111) is observed (40 min growth of graphene), which is enabled by the stitch of domain boundaries because of the well-arranged graphene nucleation orientation. These results demonstrate that the graphene layer grown on single-crystal Cu (111) also has single-crystal characteristics.

The graphene nucleation properties (5 min growth) on single-crystal Cu (111) are further evaluated by Raman mappings shown in Fig. 3(c) ~ (f), as the graphene was transferred onto a Si/SiO_2 substrate. The intensity of D band (I_D) reflecting the defect level in graphene, shows that the graphene nuclei possess a high quality (see Fig. 3(c)). As for the intensity of typical G band (I_G, see Fig. 3(d)) and 2D band (I_{2D}, see Fig. 3(e)), the corresponding graphene intensity mappings describe its nucleation density, size, and orientation, which are consistent with that measured by SEM in Fig. 3(b). The layer number of graphene is sensitive to the ratio of I_{2D} to I_G (I_{2D}/I_G), the I_{2D}/I_G with a value close to 2 proves the monolayer nature of as-grown graphene nuclei, as shown in Fig. 3(f).

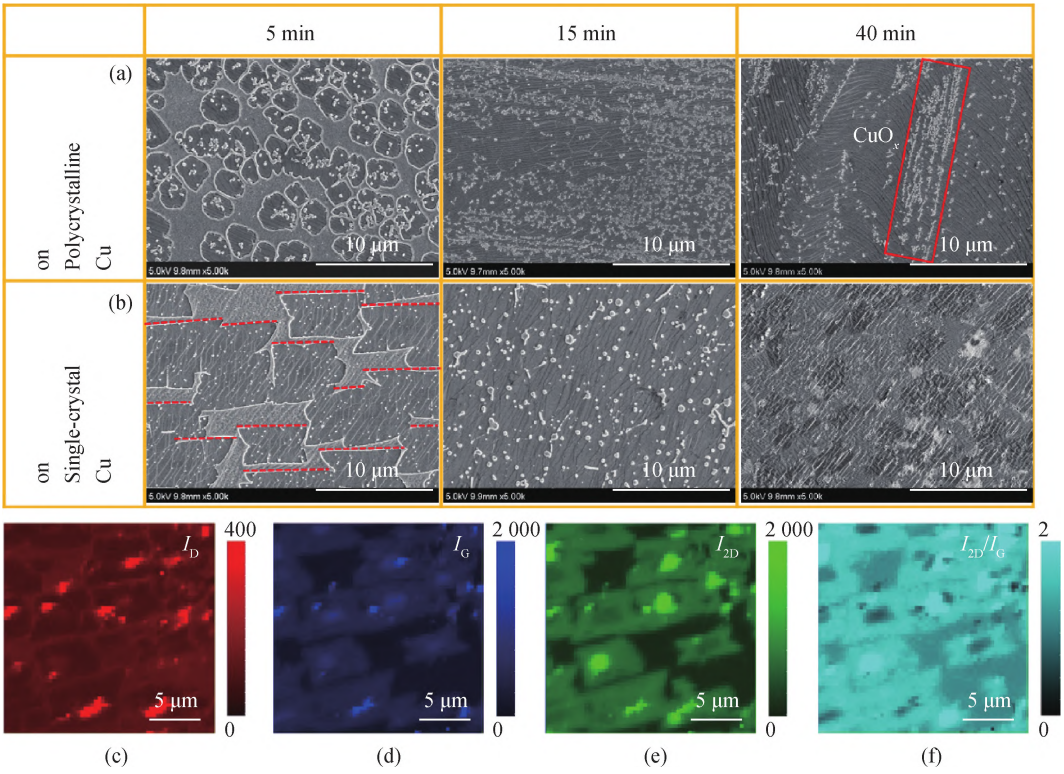

Fig. 3 Characterization of graphene nucleation and growth on polycrystalline Cu foils and single-crystal Cu (111) foils. SEM images of graphene nucleation and growth coalescence on the pristine polycrystalline Cu (a) and annealed single-crystal Cu (111) (b). The growth time of graphene is controlled at 5, 15 and 40 min. Raman mapping of the I_D(c), I_G(d), I_{2D}(e), and I_{2D}/I_G(f) for the graphene nucleation on annealed single-crystal Cu at the time of 5 min, which is transferred and measured on the Si/SiO_2 substrate

For the pristine polycrystalline Cu foils fabricated by the metallurgical cold rolling, pollution and oxidation are inevitable, which causes adverse influence on the surface morphology of as-grown graphene. As shown in Fig. 4(a) and (b), the three-dimensional (3D) AFM images of graphene (40 min growth) transferred onto Si/SiO_2 reveal a much cleaner surface morphology for that grown on the annealed single-crystal Cu (111), in which the Ra decreases from 8.78 nm (for the pristine polycrystalline Cu) to 1.41 nm. The purification of Cu foils is achieved by the high-temperature annealing process, and thus eliminating the residual pollutants on the graphene layer. The graphene resistance is positively related to the domain boundaries, and the latter hinders the transportation of free carriers. In Fig. 4(c), the sheet resistance distribution of graphene layer transferred onto Si/SiO_2 is established (20 positions are measured). The single-crystal graphene possesses lower sheet resistance with an average value of 607.5 $\Omega \cdot sq^{-1}$, and the statistic distribution is more concentrated. In contrast, the polycrystalline graphene has a high average sheet resistance of 1 415.7 $\Omega \cdot sq^{-1}$. The deduction in resistance for single-crystal graphene demonstrates its high quality.

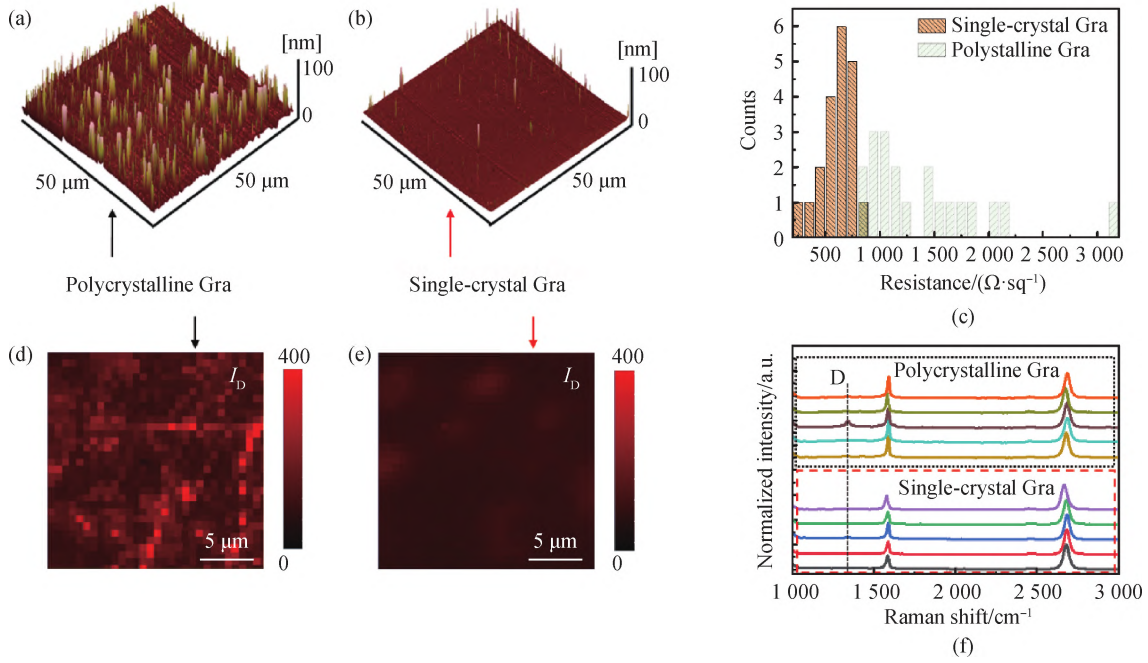

Fig. 4　Characteristics evaluation of polycrystalline graphene and single-crystal graphene transferred onto Si/SiO_2 substrate. 3D AFM images of polycrystalline graphene (a) and single-crystal graphene transferred onto the Si/SiO_2 substrate (b). (c) Statistical distribution of graphene sheet resistance. Raman mapping of I_D for the polycrystalline graphene (d) and single-crystal graphene (e). (f) Raman spectra of graphene extracted from the Raman mapping in (d) and (e)

The Raman mappings of defect-related I_D is shown in Fig. 4(d) (polycrystalline graphene) and Fig. 4(e) (single-crystal graphene), the color scale is equal as 0 ~ 400. Hence, the bright color in Fig. 4(d) represents the high-density defects in polycrystalline graphene layer. As for the single-crystal graphene layer, the I_D has been obviously decreased. These results are also confirmed by Raman spectra in Fig. 4(f), which are extracted from the Raman mapping in Fig. 4(d) and (e).

2.3　High-mobility G-FET based on single-crystal graphene

In order to further evaluate the quality of single-crystal graphene, a G-FET was constructed with the as-grown graphene as channel, and the schematic diagram of the device structure is shown in Fig. 5(a). The corresponding OM image in Fig. 5(b) identifies that the graphene channel has a length of 50 μm.

The output and transfer characteristics of the G-FET were measured at room temperature, and the plotted curves are shown in Fig. 5(c) and (d). The output curves were measured by varying the gate voltage (V_{gs}) from

0 to 80 V, showing the regulation of channel resistance by V_{gs}. The drain-source current (I_{ds}) as a function of drain-source voltage (V_{ds}) exhibits a completely linear behavior, which is typical for the G-FET with metal-graphene-semiconductor junctions, since that the graphene possesses a zero bandgap[30-32].

At the V_{ds} of 8.5 V, the transfer characteristic of G-FET in Fig. 5(d) shows a graphene Dirac point at the V_{gs} of 63.5 V, proving its p-type doping. The switch ratio and carrier mobility calculated according to the transfer characteristic curve are 145.5 and 2.31×10^3 cm^2 · V^{-1} · s^{-1}, proving the excellent performance of G-FET.

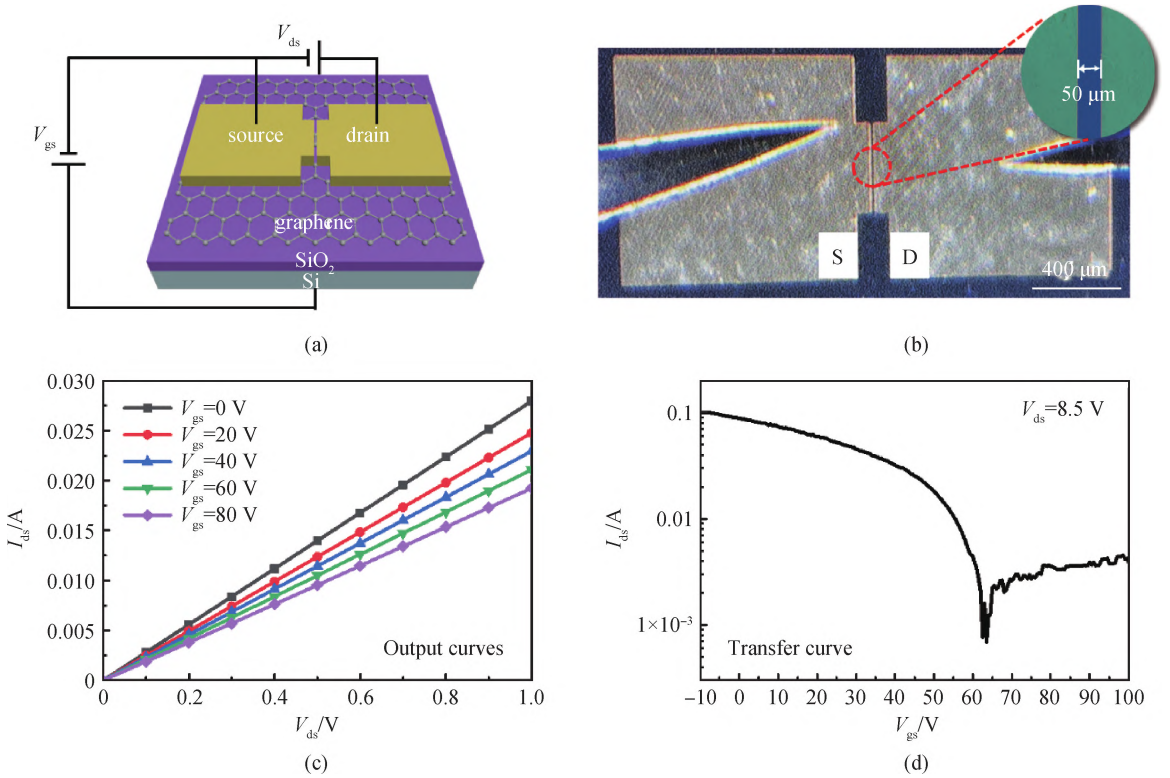

Fig. 5 Device configuration and electrical properties of G-FET. (a) Schematic diagram of G-FET device structure. (b) Top-view OM image of the G-FET. The inset is enlarged OM image of the G-FET channel. Output characteristic curves (c) and transfer characteristic curve of the G-FET (d)

3 Conclusions

We demonstrated the preparation of centimeter-size single-crystal Cu (111) by the high-temperature annealing. The dynamic investigation of Cu foils during the annealing process shows the gradual mergence of domain boundaries. The annealing of Cu foils also contributes to the deduction of 1D ridge structures, resulting in smoother surface and later nucleation regulation of graphene. As a comparison with pristine polycrystalline Cu foils, the graphene layer grown on annealed Cu (111) substrate exhibits a single-crystal nature with stitched domain boundaries, low-density defects, clean surface, and enhanced electrical conductivity. The single-crystal graphene was applied to fabricate G-FET, and achieved a high switch ratio and fine carrier mobility, further confirming the high quality of as-grown graphene layer. This work provides an efficient method for fast preparation of single-crystal catalytic Cu substrate and obtaining high-quality graphene layer, which would also be extended into other 2D materials, e.g., h-BN, triggering the advances of atomic thin-film optoelectronic and electronic devices.

References

[1] NOVOSELOV K S, GEIM A K, MOROZOV S V, et al. Electric field effect in atomically thin carbon films[J]. Science, 2004, 306(5696): 666-669.

[2] LIU F, MING P B, LI J. *Ab initio* calculation of ideal strength and phonon instability of graphene under tension[J]. Physical Review B, 2007, 76(6): 064120.

[3] MOROZOV S V, NOVOSELOV K S, KATSNELSON M I, et al. Giant intrinsic carrier mobilities in graphene and its bilayer[J]. Physical Review Letters, 2008, 100(1): 016602.
[4] NOVOSELOV K S, FAL'KO V I, COLOMBO L, et al. A roadmap for graphene[J]. Nature, 2012, 490(7419): 192-200.
[5] GEIM A K. Nobel lecture: random walk to graphene[J]. Reviews of Modern Physics, 2011, 83(3): 851-862.
[6] NOVOSELOV K S. Graphene: materials in the Flatland (Nobel lecture)[J]. Angewandte Chemie, 2011, 50(31): 6986-7002.
[7] NOVOSELOV K S, JIANG D, SCHEDIN F, et al. Two-dimensional atomic crystals[J]. Proceedings of the National Academy of Sciences of the United States of America, 2005, 102(30): 10451-10453.
[8] BLAKE P, BRIMICOMBE P D, NAIR R R, et al. Graphene-based liquid crystal device[J]. Nano Letters, 2008, 8(6): 1704-1708.
[9] HERNANDEZ Y, NICOLOSI V, LOTYA M, et al. High-yield production of graphene by liquid-phase exfoliation of graphite[J]. Nature Nanotechnology, 2008, 3(9): 563-568.
[10] COLEMAN J N, LOTYA M, O'NEILL A, et al. Two-dimensional nanosheets produced by liquid exfoliation of layered materials[J]. Science, 2011, 331(6017): 568-571.
[11] LI M, ZHOU S S, WANG R Y, et al. *In situ* formed nanoparticle-assisted growth of large-size single crystalline h-BN on copper[J]. Nanoscale, 2018, 10(37): 17865-17872.
[12] LI X S, CAI W W, AN J, et al. Large-area synthesis of high-quality and uniform graphene films on copper foils[J]. Science, 2009, 324(5932): 1312-1314.
[13] BAE S, KIM H, LEE Y, et al. Roll-to-roll production of 30-inch graphene films for transparent electrodes[J]. Nature Nanotechnology, 2010, 5(8): 574-578.
[14] WU Y P, CHOU H, JI H X, et al. Growth mechanism and controlled synthesis of AB-stacked bilayer graphene on Cu-Ni alloy foils[J]. ACS Nano, 2012, 6(9): 7731-7738.
[15] RUT'KOV E V, AFANAS'EVA E Y, PETROV V N, et al. Fabrication of graphene and graphite films on the Ni(111) surface[J]. Technical Physics, 2016, 61(11): 1724-1728.
[16] SUN J, NAM Y, LINDVALL N, et al. Growth mechanism of graphene on platinum: surface catalysis and carbon segregation[J]. Applied Physics Letters, 2014, 104(15): 152107.
[17] WANG Q, WEI L, SULLIVAN M, et al. Graphene layers on Cu and Ni (111) surfaces in layer controlled graphene growth[J]. RSC Advances, 2013, 3(9): 3046-3053.
[18] YANG S Y, ZHANG J X, CHI M Y, et al. Excellent superelasticity of Cu-Al-Mn-Cr shape memory single crystal obtained only through annealing cast polycrystalline alloy[J]. Scripta Materialia, 2019, 165: 20-24.
[19] JIN S, HUANG M, KWON Y, et al. Colossal grain growth yields single-crystal metal foils by contact-free annealing[J]. Science, 2018, 362(6418): 1021-1025.
[20] WU M H, ZHANG Z B, XU X Z, et al. Seeded growth of large single-crystal copper foils with high-index facets[J]. Nature, 2020, 581(7809): 406-410.
[21] LI L, MA T, YU W, et al. Fast growth of centimeter-scale single-crystal copper foils with high-index planes by the edge-incision effect[J]. 2D Materials, 2021, 8(3): 035019.
[22] XU X Z, ZHANG Z H, DONG J C, et al. Ultrafast epitaxial growth of metre-sized single-crystal graphene on industrial Cu foil[J]. Science Bulletin, 2017, 62(15): 1074-1080.
[23] CHEN Y, ZHANG N, LI Y F, et al. Microscale-patterned graphene electrodes for organic light-emitting devices by a simple patterning strategy[J]. Advanced Optical Materials, 2018, 6(13): 1701348.
[24] GROOVER M P. Fundamentals of modern manufacturing: materials, processes and systems[M]. Wiley: Hoboken, NJ, 2019.
[25] LUO D, CHOE M, BIZAO R A, et al. Folding and fracture of single-crystal graphene grown on a Cu(111) foil[J]. Advanced Materials, 2022, 34(15): 2110509.
[26] SRIDHARA K, FEIGELSON B N, WOLLMERSHAUSER J A, et al. Electrochemically prepared polycrystalline copper surface for the growth of hexagonal boron nitride[J]. Crystal Growth & Design, 2017, 17(4): 1669-1678.
[27] CHO J Y, MIRPURI K, LEE D N, et al. Texture investigation of copper interconnects with a different line width[J]. Journal of Electronic Materials, 2005, 34(1): 53-61.
[28] ROBINSON Z R, TYAGI P, MURRAY T M, et al. Substrate grain size and orientation of Cu and Cu-Ni foils used for the growth of graphene films[J]. Journal of Vacuum Science & Technology A, 2012, 30(1): 011401.
[29] SONG L, CI L J, LU H, et al. Large scale growth and characterization of atomic hexagonal boron nitride layers[J]. Nano Letters, 2010, 10(8): 3209-3215.
[30] XIA F N, FARMER D B, LIN Y M, et al. Graphene field-effect transistors with high on/off current ratio and large transport band gap at room temperature[J]. Nano Letters, 2010, 10(2): 715-718.

(下转第 2013 页)

(DFT-D) for the 94 elements H-Pu[J]. The Journal of Chemical Physics, 2010, 132(15): 154104.

[22] NOSÉ S. A unified formulation of the constant temperature molecular dynamics methods[J]. The Journal of Chemical Physics, 1984, 81(1): 511-519.

[23] MARTYNA G J, KLEIN M L, TUCKERMAN M. Nosé-Hoover chains: the canonical ensemble via continuous dynamics[J]. The Journal of Chemical Physics, 1992, 97(4): 2635-2643.

[24] RAMASUBRAMANIAM A. Large excitonic effects in monolayers of molybdenum and tungsten dichalcogenides[J]. Physical Review B, 2012, 86(11): 115409.

[25] PISONI R, DAVATZ T, WATANABE K, et al. Absence of interlayer tunnel coupling of K-valley electrons in bilayer MoS_2[J]. Physical Review Letters, 2019, 123(11): 117702.

[26] MOTT N F. The theory of crystal rectifiers[J]. Proceedings of the Royal Society of London Series A Mathematical and Physical Sciences, 1939, 171(944): 27-38.

[27] PENG R, MA Y D, ZHANG S, et al. Self-doped p-n junctions in two-dimensional In_2X_3 van der Waals materials[J]. Materials Horizons, 2020, 7(2): 504-510.

[28] WU Q S, XU W W, QU B Y, et al. Au_6S_2 monolayer sheets: metallic and semiconducting polymorphs[J]. Materials Horizons, 2017, 4(6): 1085-1091.

[29] YOUSEFI M, FARAJI M, ASGARI R, et al. Effect of boron and phosphorus codoping on the electronic and optical properties of graphitic carbon nitride monolayers: first-principle simulations[J]. Physical Review B, 2018, 97(19): 195428.

(上接第 1988 页)

[31] DENG T, ZHANG Z H, LIU Y X, et al. Three-dimensional graphene field-effect transistors as high-performance photodetectors[J]. Nano Letters, 2019, 19(3): 1494-1503.

[32] JMAI B, SILVA V, MENDES P M. 2D electronics based on graphene field effect transistors: tutorial for modelling and simulation[J]. Micromachines, 2021, 12(8): 979.